Beam Switching for Intra- and Inter-cell Mobility in mmWave Networks

Ayah Abusara[1], Hesham ElSawy[2], Hossam S. Hassanein[2], Aboelmagd Noureldin[3] and Akram Bin Sediq[4]

[1]Electrical and Computer Eng. Dept., Queen's University, Kingston, Canada
[2]School of Computing, Queen's University, Kingston, Canada
[3]Electrical and Computer Eng. Dept., Royal Military College of Canada, Kingston, Canada
[4]Ericsson, Ottawa, Canada

***Abstract*—This paper studies the impact of intra- and inter-cell mobility on mmWave networks with a specific focus on beam switching. The paper utilises a geometric model to partition the coverage area of a mmWave gNB cell into radial and angular sectors, thus accounting for the coverage footprints of planar antenna arrays with azimuth-tilt beam orientations (i.e., horizontal and vertical orientations). Using this model, intra-cell beam switching rate is derived analytically. We extrapolate the analysis using stochastic geometry to address inter-cell mobility and system-level beam switching. Our study establishes a relationship between the shape of the antenna array pattern and the beam switching rate. We validate our analysis via extensive Monte Carlo simulations and the results reveal the significant impact of the antenna configuration on beam switching rate. Even when the number of beams remains the same, the beam switching rate can almost double depending on how the antenna array elements are arranged.**

***Index Terms*—Millimeter Wave, Beam Switching, Geometric Analysis, Stochastic Geometry**

I. Introduction

It is the abundant untapped bandwidth available at millimeter wave (mmWave) frequencies, which holds the greatest potential to realize the ambitious speed, latency and capacity targets of Next Generation Cellular Networks (NGCN). Since the introduction of beamforming and massive multiple-input multiple-output (massive MIMO) technologies for advancing cellular networks, the interest in exploiting the mmWave band, ranging between *30-300 GHz*, has been bolstered [1]. Beamforming and massive MIMO can counter the shortcomings of mmWave and enable a wide-area coverage for mmWave networks. In addition, these technologies are capable of focusing the range-limited mmWave signals into directional beams, achieving improved spatial selectivity and a link-budget viable for use in cellular networks [2], [3]. In addition to extending the range of mmWave signals and improving their propagation characteristics, highly directional beams can also minimize intra-cell interference and enhance spectral efficiency [4].

However, beam-based communication imposes challenges on network control and management. The smaller footprint of directional beams entails frequent beam switches for mobile devices, which results in excessive service interruptions and control signaling overheads. In addition, beam-based communication is prone to abrupt channel variations due to blockages, misalignment and failures, which can be further exacerbated under user mobility [4], [5].

In NGCN, user mobility can be classified into intra-cell and inter-cell mobility, also known as beam-level and cell-level mobility, respectively. Intra-cell mobility refers to the movement of a user within a single gNodeB (gNB) using beamformed mmWave communication. On the other hand, inter-cell mobility describes user movement between different gNBs. In this paper, we investigate beam switching function for both classes of mobility. As specified by the 3rd Generation Partnership Project (3GPP), beam switching is a beam management function to adjust the orientation of an antenna array pattern to maintain effective communication with mobile users [5], [6].

Few studies have investigated the incurred costs of frequent beam switching on network functions and the user experience. For example, the study in [7] suggests filtering signal strength measurements for beams prior to beam switching decisions to enhance beam switching performance. In [8], beam switching sensitivity under filtering and parametrization is investigated. The authors in [4] and [9] develop a mathematical framework to model beam switching and conduct a system-level analysis using stochastic geometry. However, there exists major caveats in beam switching studies in the literature, where current research [4], [8], [10] approximates beamforming models using a sectorized circle that captures horizontal coverage of beams in the azimuth plane. Whereas, practical antenna array patterns can adapt beams in both the azimuth and tilt, also known as elevation, planes [3], [11].

This paper uses a beamforming model based on planar antenna array patterns to explore how beam switching affects mobile users. To the best of our knowledge, this is the first attempt to rigorously capture beam coverage for beam switching, considering a practical beamforming system with a planar antenna array covering the azimuth and tilt directions. The developed model utilizes a geometry-based beam switching analysis within a single cell (i.e., for intra-cell mobility). The utilized geometry-based analysis is not only more realistic than prior research work, but is also more tractable. In this paper, the beam switching rate is linked to the shape of the antenna array pattern for the first time. Taking into account our beam footprint coverage model, stochastic geometry is employed to

ICC 2024 - IEEE International Conference on Communications | 978-1-7281-9054-9/24/$31.00 ©2024 IEEE | DOI: 10.1109/ICC51166.2024.10622895

extrapolate the analysis to assess system-level beam-switching performance for inter-cell mobility.

- We propose a mathematical model that captures a realistic beam coverage with respect to the 2D space. The model approximates the beam coverage for an intricate planar antenna array pattern using angular and radial sectors.
- The proposed model yields an expression for the beam switching rate for any number of beams supported by a planar antenna array using fundamental geometric principles.
- An expression for system-level beam switching rate is also derived using stochastic geometry.

The remainder of the paper is organized as follows. Section II provides an overview of beam coverage, beam switching and our analytical model. Section III describes our analytical approach and findings. Section IV presents the results of our simulations. Conclusions and future work are presented in Section V.

II. System Model

The aim of this paper is to assess the rate of beam switching for intra- and inter-cell mobility, that is evaluating the beam switching experienced by a user equipment (UE) as it travels within a single typical cell and across different cells in the network.

A. Beam Coverage Footprint

To model and analyze beam switching in the context of NGCN, it is essential to understand the coverage footprint of beam-based mmWave networks and their impact on user mobility. Coverage in mmWave networks differs from omnidirectional legacy microwave networks, as illustrated in Fig. 1. Omnidirectional antennas provide distance-based coverage, whereas in beam-based communication, the coverage is distance and direction dependent [1].

Coverage in beamformed communication is measured by bursts of synchronization signal blocks (SSB) that are periodically transmitted to users present in the area, where each block represents a beam pointing in a specific direction in the 2D space [5], [6]. A key feature that characterizes the spatial coverage of a realistic beam pattern is the antenna geometry, which determines the number of antenna elements at the gNB and the directions covered by those elements [2], [3]. Based on its geometry, the antenna array pattern can be categorized into a uniform linear array (ULA) or a uniform planar array (UPA) [2], [12]. The main difference between the two layouts is that the ULA is a one-dimensional antenna array that has $N_h \times 1$ size, while the UPA is a two-dimensional antenna array that has the size $N_h \times N_v$, where N_h and N_v are the numbers of antenna elements in the horizontal and vertical directions, respectively [12]. Most theoretical beamforming literature fail to draw a distinction between the two structures and just assumes ULA antennas with angular sectors coverage, for their tractability and ease of analysis [12], as depicted in Fig. 1b.

Nevertheless, UPAs are more popular for practical deployment in NGCN as they pack a greater number of antenna elements [12], [13]. In addition, UPAs can adopt beams in the azimuth and tilt directions, making it possible to perform 3D beamforming, which ensures higher precision coverage wherever the user may be [2], [12], [13]. Motivated by the facts mentioned above, we propose using a more generic coverage model, where beams can point in the azimuth and tilt directions along the horizontal and vertical planes. Given the antenna geometry for a UPA, the footprint associated with each beam has angular and radial borders in the 2D space. Together, beams form a grid of footprints covering the cell area, as shown in Fig. 1c.

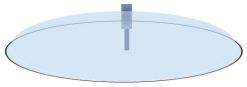

(a) Omnidirectional antenna coverage

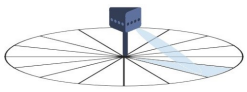

(b) Angular beam coverage model

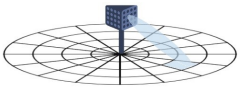

(c) Angular-radial beam coverage model

Fig. 1: Omnidirectional antenna coverage footprint vs. beams footprint

III. Beam Switching Analysis

We adopt an analysis approach wherein we analyze the average number of beam switches initially within a single cell and then extrapolate our analysis to the network-level.

A. Intra-cell Mobility and Beam Switching Rate

Beam switching occurs when the user moves out from the coverage area of a beam into another. To evaluate beam switching for intra-cell mobility, we focus on a single gNB with a circular coverage area, which is partitioned into $n \times m$ beam footprints, where $n \in \mathbb{N}$ is the number of angular sectors and $m \in \mathbb{N}$ is the number of radial sectors formed by the antenna pattern at the gNB. Let T denote the segment of the UE trajectory passing through a single cell, where T is a straight line, randomly oriented and of a finite length $0 \leq \mid T \mid \leq 2r$, and r is the cell radius. Let A denote the coverage footprint of any beam in the cell, and ∂A denote the set of beam borders in a single cell. To study the effect of beam switching, we find the number of intersections between the user trajectory and the beam boundaries, denoted by $N\{T \cap \partial A\}$. The average number of intersections between

a random user trajectory and the beam boundaries in a cell is denoted by $\mathbb{E}[N\{T \cap \partial A\}]$. For tractability, we decompose the average beam switching for the combined angular and radial borders into angular and radial sectors switching separately $\partial A = \partial A_{angular} + \partial A_{radial}$, as shown in Fig. 2. The average number of beam switches is derived by adding up the individual contributions of both types of boundaries into the total average beam switching, in the sense that $\mathbb{E}[N\{T \cap \partial A\}] = \mathbb{E}[N\{T \cap \partial A_{angular}\}] + \mathbb{E}[N\{T \cap \partial A_{radial}\}]$. The derivations of the average switching for the two types of boundaries are tractable using geometry analysis, as detailed in the next subsections.

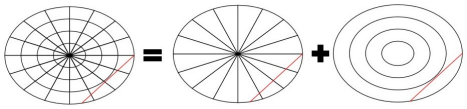

Fig. 2: Beam boundaries are decomposed into angular and radial sector boundaries

1) Deriving The Average Switching for Angular Sectors: it is important to note that the average switching for angular sectors is the average beam switching for a ULA antenna pattern or the conventional angular beam coverage model, shown in Fig. 1b. Next, we present a derivation for $\mathbb{E}[N\{T \cap \partial A_{angular}\}]$. Since $\partial A_{angular}$ is a constant representing the number of angular sectors n, the only random variable in the problem is the user trajectory T. Hence, the average sectors switching can be approximated by evaluating the number of sector switches for an average length trajectory $\mathbb{E}[T]$.

Lemma 1: By employing geometric principles, we derive an expression for the average angular sector switches:

$$\mathbb{E}[N\{T \cap \partial A_{angular}\}] = \left\lceil \frac{n \sin^{-1}(\frac{2}{\pi})}{\pi} \right\rceil. \tag{1}$$

Proof: the proof is given in Appendix A.

2) Deriving The Average Switching for Radial Sectors: following a similar approach to the previous analysis, we derive the average number of switches for radial sectors $\mathbb{E}[N\{T \cap \partial A_{radial}\}]$. Again, the radial boundaries ∂A_{radial} for a particular cell is a constant that represents the number of radial sectors m.

Lemma 2: Through geometric and probability tools, we drive an expression for the average number of radial sector switching:

$$\mathbb{E}[N\{T \cap \partial A_{radial}\}] = \frac{4}{\pi} \sum_{k=0}^{m-1} (m-k)[\cos^{-1}(\frac{k}{m}) - \cos^{-1}(\frac{k+1}{m})]. \tag{2}$$

Proof: the proof is given in Appendix B.

Based on the above analysis, the overall average beam switching for a UPA, see Fig. 2, is given by:

$$\mathbb{E}[N\{T \cap \partial A\}] = \left\lceil \frac{n \sin^{-1}(\frac{2}{\pi})}{\pi} \right\rceil + \frac{4}{\pi} \sum_{k=0}^{m-1} (m-k)[\cos^{-1}(\frac{k}{m}) - \cos^{-1}(\frac{k+1}{m})] - 1. \tag{3}$$

Note, we subtract a 1 from the overall average beam switching expression to remove a point of intersection with the cell boundary when the user moves outside the cell, as this point does not contribute to intra-cell beam switching. We can derive the beam switching rate (BSR), from the average beam switching $\mathbb{E}[N\{T \cap \partial A\}]$. The BSR measures the number of beam switching events per unit time throughout the user's travel. Let v equal the user speed and $\mid T \mid$ is the length of the user trajectory, then we can evaluate BSR as:

$$\text{BSR} = \frac{\mathbb{E}[N\{T \cap \partial A\}]}{\mid T \mid} \times v. \tag{4}$$

Note, $\frac{\mathbb{E}[N\{T \cap \partial A\}]}{|T|}$ represents the linear beam switching intensity for a single cell, usually referred to as μ.

B. Inter-cell Mobility and Beam Switching Rate

In order to evaluate system-level beam switching for inter-cell mobility, our study considers a cellular network with spatially distributed gNBs according to a homogeneous Poisson point process (PPP) $\Phi \subset \mathbb{R}^2$ with intensity λ. This random process partitions the space into cells forming a Poisson-Voronoi tessellation, where each cell has $n \times m$ distinct beam footprints, as shown in Fig. 3. Let L denote the UE trajectory passing through the network. Following the same assumption in Section III-A, we assume L is a straight line and of a finite length. The PPP is an isotropic and stationary process, so L can be any fixed straight line, regardless of its orientation.

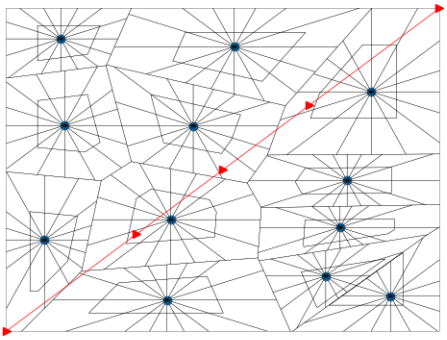

Fig. 3: Angular-radial beam boundaries for a PPP network

Let $X \in \Phi$ denote the positions of the gNBs in the network. The set of cell boundaries composing the Poisson-Voronoi tessellation can be defined as:

$$\partial X = \left\{ x \in \mathbb{R}^2 | \exists \{x_1, x_2\} \subset \Phi, s.t. |x - x_1| = |x - x_2| \right\}. \tag{5}$$

Note that cell switching occurs at the points of intersection between the user trajectory L and ∂X. Following the analysis in [14], ∂X is a stationary and isotropic fibre process generated by Φ, hence the expected number of intersections between L and ∂X, is given by:

$$\mathbb{E}[N\{L \cap \partial X\}] = \frac{2}{\pi}\mu_1(\partial X)\,|L|_1\,, \tag{6}$$

where $|L|_1$ is the Lebesgue measure on the line L (i.e., the length of L), and $\mu_1(\partial X)$ is the length intensity of the fibre process ∂X, which is the expected length of ∂X in a unit square:

$$\mu_1(\partial X) = \mathbb{E}[\Big|\partial X \cap [0,1)^2\Big|_1]. \tag{7}$$

We know from [15], that the length intensity for a Poisson-Voronoi is equal to $2\sqrt{\lambda}$. Therefore, the average number of intersections between the user trajectory and the cell borders (i.e., average number of cell switches):

$$\mathbb{E}[N\{L \cap \partial X\}] = \frac{4\sqrt{\lambda}}{\pi}\,|L|_1\,. \tag{8}$$

To obtain the average number of beam switching for intra and inter-cell mobility, we superimpose the average number of beam switches corresponding to a single cell (i.e., intra-cell mobility) in (3) to the linear intensity of cell switching for a PPP network. Hence, the system-level beam switching is obtained as follows:

$$\begin{aligned}\mathbb{E}[N\{L \cap \partial X \times \partial A\}] &= \frac{4\sqrt{\lambda}}{\pi}\mathbb{E}[N\{L \cap \times \partial A\}]\,|L|_1 \\ &= \frac{4\sqrt{\lambda}}{\pi}\Bigg(\left\lceil \frac{n\sin^{-1}(\frac{2}{\pi})}{\pi}\right\rceil + \\ &\frac{4}{\pi}\sum_{k=0}^{m-1}(m-k)[\cos^{-1}(\frac{k}{m}) - \cos^{-1}(\frac{k+1}{m})] - 2\Bigg)\,|L|_1\,.\end{aligned} \tag{9}$$

Note in (9), we subtract 2 from the average beam switching expression to avoid double counting intersections at the cell boundary. Following the same step as (4), the system-level linear beam switching intensity and BSR are evaluated. Considering the case when the number of angular sectors (i.e., the number of beams in a conventional model) is restricted to 2^k with $k \in \mathbb{N}$, see the work in [4], the average number of intra-cell beam switches in (3) can be approximated as 2^{k-2}. To find the overall system-level linear beam switching intensity, we multiply the intra-cell average beam switching by the cell switching intensity in (8) which gives $\frac{2^k\sqrt{\lambda}}{\pi}$. This matches the derived system-level linear beam switching intensity for the special case adopted in [4].

IV. Results and Discussions

A. Simulation Results: Intra-cell Mobility

To further demonstrate our analysis, we used the Shapley Python© package, in [16], to simulate cells with various numbers of angular and radial sectors. In each round of the simulation, a random user trajectory is created and the number of intersections with the angular and radial boundaries is recorded. The average number of intersections is then calculated and plotted against the analytically derived averages, as shown in Fig. 4. As depicted, our analysis matches the simulation with great accuracy. In addition, it is important to note that the average switching contribution from radial sectors (i.e., tilt domain) is greater than that of angular sectors; hence, ignoring the radial sectors and utilizing the conventional beam coverage model underestimates the average number of beam switches for realistic antenna array patterns.

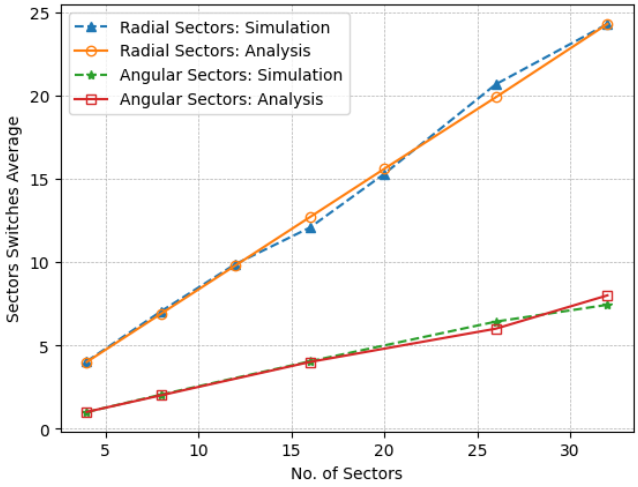

Fig. 4: The simulated vs. analytical average number of switches for different number of sectors

Similar results are also obtained for the combined average beam switching, as shown in Fig. 5. The average beam switching is calculated via simulations for different angular and radial sectors combinations and plotted against the analytically derived average beam switching. Results show that the simulations confirm the accuracy of our analysis. Moreover, results also confirm that a greater number of angular and radial sectors results in greater average beam switching.

To examine the impact of different antenna geometry designs on beam switching, we plotted the analytical average beam switching for different combinations of $angular \times radial$ sectors, while keeping the number of beams constant, see Fig. 6. The figure clearly shows that the average beam switching is higher when the number of radial sectors is greater than the number of angular sectors. From these results, it means that antenna arrays with larger degrees of freedom in steering beams in the tilt domain result in a larger beam switching average. There are fewer average beam switches when square antenna configurations are used, while the beam switching average is reduced nearly by half when horizontal azimuth coverage is greater than tilt coverage (i.e., a greater number of angular sectors is used). This result confirms that not only is the beam switching performance dependant on the sheer number of beams at a gNB, but also their spatial distribution in the coverage area.

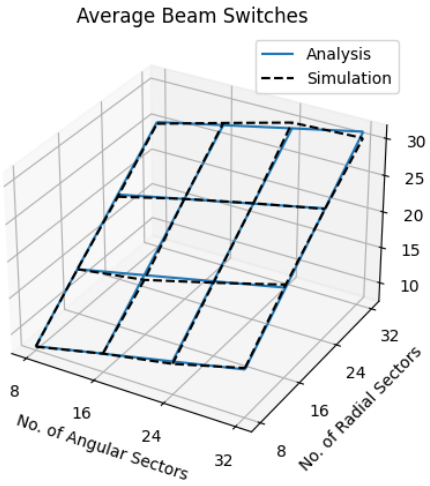

Fig. 5: The average beam switching for different combinations of angular vs. radial sectors

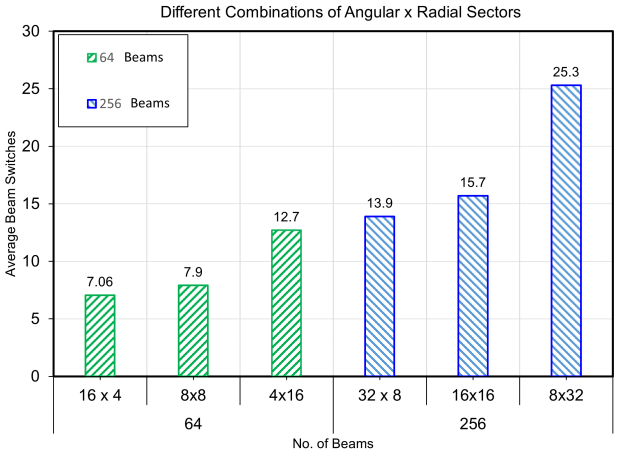

Fig. 6: The effect of different antenna designs on beam switching

B. Simulation Results: Inter-cell Mobility

To validate our analysis for the system-level linear beam switching intensity, we simulate a cellular network on a $10 \times 10\ km^2$ area. With each run of the simulation, gNBs in the network are randomly distributed and the number of beam switches taking place for a fixed user trajectory is evaluated. For every examined scenario, results are averaged and plotted in Fig. 7. The beam switching intensity is studied for different network gNB intensities λ and for different antenna array patterns per gNB. The results show a similar trend as in inter-cell mobility but on a larger scale. That is the shape of the antenna array $angular \times radial$ has an important effect on the beam switching intensity. For instance, the beam pattern $8 \times 3 = 24$ achieves a fewer BSR than $16 \times 1 = 16$ although it holds a greater number of beams. According to the results, the analysis and simulation for conventional angular models are almost exact, while they have a small offset for angular-radial beam coverage models. In addition, Fig. 7 illustrates that increasing the network density λ, the beam switching intensity also increases.

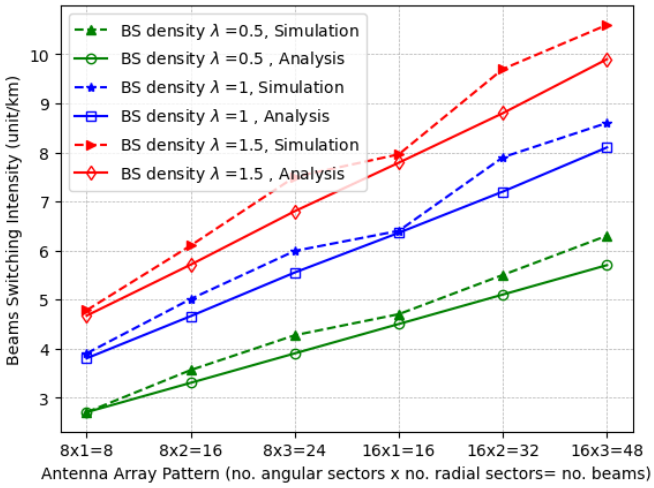

Fig. 7: System-level linear beam switching intensity for different antenna array patterns and different λ

V. Conclusion

In this paper, we proposed a mathematical model to capture the beam coverage for a realistic planar beamforming antenna array. We used a circular model with angular and radial sectors to account for beam boundaries in a single cell and explored their impact on the intra-cell mobility of users. A closed-form expression for BSR is derived, using fundamental geometric principles. The analytical expression for the BSR is validated using simulations. Beam switching results were obtained for different combinations of angular and radial sectors. Our analysis demonstrated the effect of different designs of antenna configurations on the beam switching performance. The paper also employed stochastic geometry to extend the analysis to a system-level analysis and study the effect of beam switching on inter-cell mobility. An analytical expression for system-level beam switching is derived and validated using simulations. Future work will examine and compare power measurement-based beam switching to geometry-based beam switching discussed in this paper.

References

[1] C. K. Armeniakos and A. G. Kanatas, "Angular Distance-Based Performance Analysis of mmWave Cellular Networks," in *IEEE Global Communications Conference*, 2022, pp. 5432–5437.

[2] M. Giordani, M. Polese, A. Roy, D. Castor, and M. Zorzi, "A Tutorial on Beam Management for 3GPP NR at mmWave Frequencies," *IEEE Communications Surveys Tutorials*, vol. 21, no. 1, pp. 173–196, 2019.

[3] W. Kong, Y. Hu, J. Li, L. Zhang, and W. Hong, "2-D Orthogonal Multibeam Antenna Arrays for 5G Millimeter-Wave Applications," *IEEE Transactions on Microwave Theory and Techniques*, vol. 70, no. 5, pp. 2815–2824, 2022.

[4] S. S. Kalamkar, F. Baccelli, F. M. Abinader, A. S. M. Fani, and L. G. U. Garcia, "Beam Management in 5G: A Stochastic Geometry Analysis," *IEEE Transactions on Wireless Communications*, vol. 21, no. 4, pp. 2275–2290, 2022.

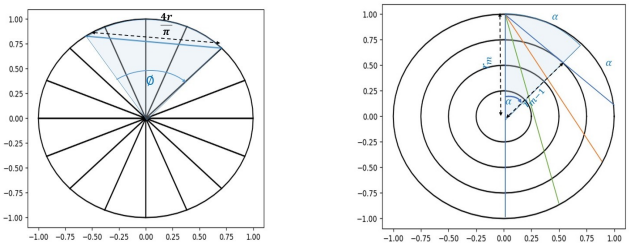

(a) The number of angular sector switches by an average length chord

(b) The average number of radial sector switches by a chord

Fig. 8: Derivation of the average number of angular and radial sectors switching

[5] A. Kose, H. Lee, C. H. Foh, and M. Dianati, "Beam-Based Mobility Management in 5G Millimetre Wave V2X Communications: A Survey and Outlook," *IEEE Open Journal of Intelligent Transportation Systems*, vol. 2, pp. 347–363, 2021.

[6] M. Tayyab, X. Gelabert, and R. Jäntti, "A Survey on Handover Management: From LTE to NR," *IEEE Access*, vol. 7, pp. 118 907–118 930, 2019.

[7] U. B. Elmali, A. Awada, U. Karabulut, and I. Viering, "Analysis and Performance of Beam Management in 5G Networks," in *International Symposium on Personal, Indoor and Mobile Radio Communications (PIMRC)*, 2019, pp. 1–7.

[8] F. Fernandes, C. Rom, J. Harrebek, and G. Berardinelli, "Beam Management in mmWave 5G NR: an Intra-Cell Mobility Study," in *93rd Proc. IEEE Veh. Tech. Conf. (VTC)*, 2021, pp. 1–7.

[9] W. Chen, L. Li, Z. Chen, H. H. Yang, and T. Q. Quek, "Mobility and Blockage-induced Beam Misalignment and Throughput Analysis for THz Networks," in *IEEE Global Communications Conference*, 2021, pp. 1–6.

[10] F. Baccelli, B. Liu, L. Decreusefond, and R. Song, "A User Centric Blockage Model for Wireless Networks," *IEEE Transactions on Wireless Communications*, vol. 21, no. 10, pp. 8431–8440, 2022.

[11] M. Rebato, L. Resteghini, C. Mazzucco, and M. Zorzi, "Study of Realistic Antenna Patterns in 5G mmWave Cellular Scenarios," in *IEEE International Conference on Communications (ICC)*, 2018, pp. 1–6.

[12] N. T. Nguyen, J. Kokkoniemi, and M. Juntti, "Beam Squint Effects in THz Communications with UPA and ULA: Comparison and Hybrid Beamforming Design," in *IEEE Globecom Workshops*, 2022, pp. 1754–1759.

[13] Y.-N. R. Li, B. Gao, X. Zhang, and K. Huang, "Beam Management in Millimeter-Wave Communications for 5G and Beyond," *IEEE Access*, vol. 8, pp. 13 282–13 293, 2020.

[14] S. N. Chiu, D. Stoyan, W. S. Kendall, and J. Mecke, *Stochastic Geometry and its Applications*, 3rd ed. Wiley, 2013.

[15] W. Bao and B. Liang, "Stochastic Geometric Analysis of User Mobility in Heterogeneous Wireless Networks," *IEEE Journal on Selected Areas in Communications*, vol. 33, no. 10, pp. 2212–2225, 2015.

[16] Shapely 2.0.1. [Online]. Available: https://pypi.org/project/shapely/

APPENDIX A
PROOF OF LEMMA 1

In the case of a gNB with a circular coverage area, T is equivalent to a circular chord. To find the average length of T passing through the cell $\mathbb{E}[|\ T\ |]$, we need to define the $|\ T\ |$:

$$|T| = dist\left\{(r\cos\beta, r\sin\beta), (r\cos\alpha, r\sin\alpha)\right\}, \tag{10}$$

it follows from the cosine rule for isosceles triangle that this distance is equal to

$$|T| = \sqrt{2}r\sqrt{1-\cos(\beta-\alpha)}\ , \tag{11}$$

where for any T,

$$0 \leq \alpha \leq 2\pi\ and\ 0 \leq \beta \leq 2\pi. \tag{12}$$

Then, $\mathbb{E}[|T|]$ is obtained using:

$$\begin{aligned}\mathbb{E}[|T|] &= \frac{\int_0^{2\pi}\int_0^{2\pi}\sqrt{2}r\sqrt{1-\cos(\beta-\alpha)}\ d\alpha\ d\beta}{4\pi^2} \\ &= \frac{4r}{\pi}.\end{aligned} \tag{13}$$

Given the average chord length $\mathbb{E}[|T|] = \frac{4r}{\pi}$, we can find the value of the angle ϕ which achieves this length, i.e., $\frac{4r}{\pi}$, and divide it by width of the angular sector in order to evaluate $\mathbb{E}[N\{T \cap \partial A_{angular}\}]$, see Fig. 8a. ϕ is equal to:

$$\phi = 2\sin^{-1}(\frac{2}{\pi}). \tag{14}$$

We consider the width for an angular sectors at a gNB to be $\frac{2\pi}{n}$, where n is the total number of angular sectors. To find $\mu_{angular}$, we use:

$$\mathbb{E}[N\{T \cap \partial A_{angular}\}] = \left\lceil \frac{n\phi}{2\pi} \right\rceil = \left\lceil \frac{n\sin^{-1}(\frac{2}{\pi})}{\pi} \right\rceil. \tag{15}$$

Note that the ceiling function is used to get rid of any fractions and force the number of intersections to be an integer.

APPENDIX B
PROOF OF LEMMA 2

Let r_i denote the radius of the ith radial sector in the coverage area of a gNB and $r_i = \frac{ir}{m}$, where $i = 1, 2, 3, .., m$ and m is the total number of angular sectors. The radius r_m is thus equal to r and all other radii are rational multiples of r. Note that the minimum number of points of intersection between a chord and radial borders of a gNB (i.e., ∂A_{radial}) is 2, while the maximum is $2m$. This number can increase or decrease by 2, depending on where the chord falls in the circle, as illustrated in Fig. 8b. Let Z be the number of intersection points with the radial sectors $Z \triangleq N\{T \cap \partial A_{radial}\}$. As shown in the figure, the probability that the chord T has exactly 2 points of intersection is $\frac{2\alpha}{\pi}$, which can be evaluated in terms of m as:

$$\mathbb{P}\left\{Z = 2\right\} = \frac{2\alpha}{\pi} = \frac{2\cos^{-1}(\frac{m-1}{m})}{\pi}, \tag{16}$$

similarly,

$$\mathbb{P}\{Z = 4\} = \frac{2(\cos^{-1}(\frac{m-2}{m}) - \cos^{-1}(\frac{m-1}{m}))}{\pi}. \tag{17}$$

Recursively applying the above procedure and using $\mathbb{E}[Z] = \sum Z\mathbb{P}_Z$, we can obtain $\mathbb{E}[N\{T \cap \partial A_{radial}\}]$, which is the average number of intersection points between a random chord crossing the circle and its radial borders.

$$\begin{aligned}&\mathbb{E}[N\{T \cap \partial A_{radial}\}] = \\ &\frac{4}{\pi}\sum_{k=0}^{m-1}(m-k)[\cos^{-1}(\frac{k}{m}) - \cos^{-1}(\frac{k+1}{m})].\end{aligned} \tag{18}$$